Similarities in the C_p/T^3 Peaks in Amorphous and Crystalline Metals

D. J. Safarik, R. B. Schwarz, and M. F. Hundley

Materials Science and Technology Division, Los Alamos National Laboratory, Los Alamos, New Mexico 87545, USA

(Received 16 June 2005; published 17 May 2006)

A low-temperature peak in C_p/T^3 vs T is ubiquitous to glasses. It arises from an abundance of low-frequency vibrations, the origin of which remains unclear. A comparable C_p/T^3 vs T peak is observed in crystals due to the dispersion of acoustic phonons and/or the excitation of optical phonons. We compared the C_p/T^3 vs T peaks in metallic and oxide glasses to elemental crystals by analyzing specific heat, phonon density of states, and elastic constant data. We observe no clear distinction in the peak temperature or amplitude between metallic glasses and crystals. Surprisingly, the peak is larger in single crystal $Pd_{40}Cu_{40}P_{20}$ than in glassy $Pd_{40}Cu_{40}P_{20}$.

DOI: 10.1103/PhysRevLett.96.195902 PACS numbers: 65.60.+a, 63.20.Pw

Amorphous solids have two low-temperature specific heat anomalies. The first occurs below 1 K, where the heat capacity has a linear dependence on temperature that cannot be attributed to conduction electrons [1]. This behavior has been explained in terms of an ensemble of two-level tunneling systems having a uniform distribution of energy gaps [2,3]. The second anomaly occurs above ~2 K, where glasses have a phonon heat capacity that is larger than expected based upon the Debye T^3 law [4]. This excess is usually observed as a hump in a plot of C_p/T^3 vs T that is centered at ~5–20 K.

The hump in C_p/T^3 vs T appears because glasses have an excess of low-energy vibrational states that are not accounted for by the Debye model. These modes are seen in inelastic neutron scattering [5,6]. In Raman scattering they appear as a low-frequency peak whose intensity varies with temperature according to the Bose distribution function (which has led to the name "boson" peak) [4]. Because these extra low-frequency states are observed in glasses of all bonding types (metallic, covalent, ionic, etc.) [5], they are thought to be a fundamental feature of glass dynamics.

The origin of the extra low-frequency states remains unclear. It has been suggested that they result from resonant modes involving loosely bound structural fragments [7], atom clusters [5], or strings of atoms [8], the latter identified through molecular dynamics simulations [8]. In the frequently cited soft potential model, the low-frequency vibrations, whatever their nature, are represented by soft anharmonic potential wells [9]. Other authors have modeled these modes with spatially fluctuating interatomic force constants [10]. These models are phenomenological and provide no microscopic explanation for the origin of the excitations. The interstitialcy theory [11,12] proposes a microscopic origin of the boson peak. This theory models the amorphous solid as a crystal that contains ~3–10% self-interstitials in dumbbell configurations. Here, the boson peak arises simply from the excitation of the low-frequency resonant modes of the self-interstitials.

The low-temperature lattice heat capacity of most crystalline solids also exceeds the Debye T^3 prediction [13], leading to a hump in the C_p/T^3 vs T curve that, as will be shown here, closely resembles the hump in glasses. In contrast to glasses, the origin of the C_p/T^3 vs T peak in crystals is known [13].

In view of the similarities in their C_p/T^3 vs T peaks, it is interesting to compare glasses and crystals to determine if the boson peak vibrational modes in glasses can be differentiated from low-frequency acoustic and optical modes in crystals using the specific heat data alone. We have analyzed low-temperature specific heat, phonon density of states, and elastic constant data for a variety of crystalline and glassy materials. Figure 1 shows $C_{p,\mathrm{lat}}/\beta T^3$ vs T/θ_D for several crystalline and amorphous solids. In the figure, $C_{p,\mathrm{lat}}$ is the phonon heat capacity, $\beta = 12\pi^4 R/(5\theta_D^3)$ (the Debye T^3 coefficient), θ_D is the Debye temperature, and R is the gas constant. All data were obtained from the literature, with the exception of the $Pd_{40}Cu_{40}P_{20}$ data, which is our own. Each material in Fig. 1 has a hump in its $C_{p,\mathrm{lat}}/\beta T^3$ vs T/θ_D curve in the temperature range where

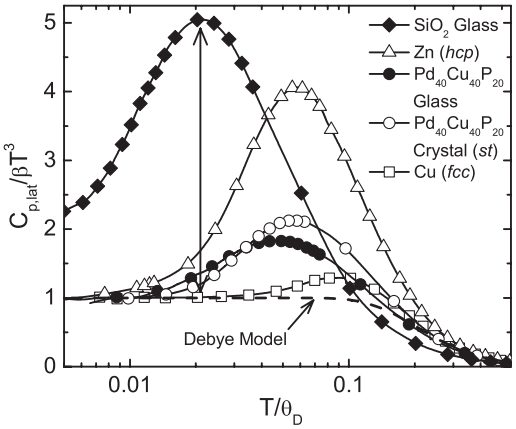

FIG. 1. $C_{p,\mathrm{lat}}/\beta T^3$ versus T/θ_D for hcp Zn [24,25], fcc Cu [25], glassy SiO_2 [4,25], simple tetragonal (*st*) $Pd_{40}Cu_{40}P_{20}$ single crystal [our data], glassy $Pd_{40}Cu_{40}P_{20}$ [our data], and the Debye model. For clarity, only selected data points are shown. The arrow defines the peak amplitude for SiO_2.

the Debye model predicts $C_{p,\mathrm{lat}}/\beta T^3$ is constant. Note that the peak amplitude is larger for the $Pd_{40}Cu_{40}P_{20}$ single crystal than for the $Pd_{40}Cu_{40}P_{20}$ glass.

Figure 2 shows the measured (solid curve) [14] and the Debye [dashed curve, $g(\omega) \propto \omega^2$] vibrational density of states (VDOS) for Cu. Most fcc and bcc crystals that lack optical modes have a VDOS spectrum similar to that shown in Fig. 2. In the range $10 < \hbar\omega < 21$ meV, the measured VDOS exceeds the Debye model prediction (horizontally hatched area, Fig. 2), whereas in the range $21 < \hbar\omega < 27$ meV, the measured VDOS is lower than the Debye model prediction (vertically hatched region). By considering the progressive excitation of phonons with increasing temperature, it is easy to visualize that the peak in the $C_{p,\mathrm{lat}}/\beta T^3$ vs T/θ_D curve corresponds to the energy where the measured and Debye VDOS cross for the first time at ~21 meV. As the temperature increases and phonons in the $10 < \hbar\omega < 21$ meV range become excited, the specific heat increases more rapidly with temperature than predicted by Debye's T^3 law. The value of $C_{p,\mathrm{lat}}/\beta T^3$ then rises above the Debye model prediction by an amount proportional to the horizontally hatched area. Excess heat capacity continues to accumulate until the temperature also excites phonons in the $21 < \hbar\omega < 27$ meV range. Once this happens, $C_{p,\mathrm{lat}}$ increases more slowly with temperature than predicted by the Debye T^3 law, and $C_{p,\mathrm{lat}}/\beta T^3$ decreases [15].

The abrupt changes in the VDOS in Fig. 2 are van Hove singularities, which denote critical points in reciprocal space where a dispersion curve has zero slope ($d\omega/dK = 0$) and the corresponding lattice wave is nonpropagating [16]. Some (but possibly not all) such critical points are located at high symmetry points at the boundaries of the first Brillouin zone [17]. The down-pointing arrows in Fig. 2 denote frequencies where $d\omega/dK = 0$, which we obtained from the phonon dispersion curves for Cu [14]. Only selected critical points are indicated. Each arrow is associated with a propagation direction (in brackets) and a polarization direction ($T \equiv$ Transverse, $L \equiv$ Longitudinal).

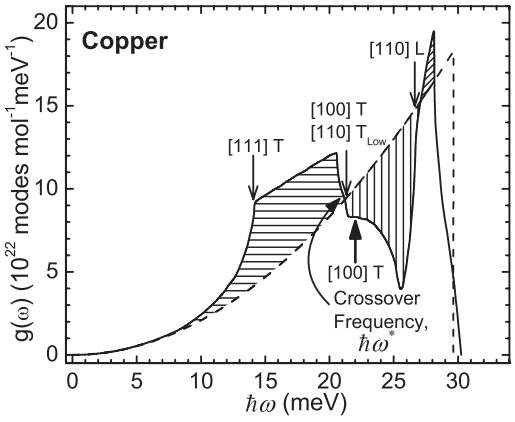

FIG. 2. Experimental (solid line, [14]) and Debye (dashed line) VDOS for Cu. The significance of the downward and upward pointing arrows is described in the text.

Of special interest here is the singularity at the crossover frequency $\hbar\omega^* \sim 21$ meV. As exemplified in Fig. 2, $\hbar\omega^*$ for fcc elements corresponds to the Brillouin zone boundary frequency for the two shear waves in the [100] direction and the low velocity shear wave in the [110] direction. For bcc elements, $\hbar\omega^*$ corresponds to the Brillouin zone boundary frequency for shear waves in the [100] and the [111] directions. By analogy with cubic crystals, in hcp and trigonal crystals $\hbar\omega^*$ is expected to correspond to the zone boundary frequency for the fast shear wave in the [100] direction.

The dispersion curve for a given acoustic branch and propagation direction can be approximated using the Born–von Kármán model for a linear chain of atoms,

$$\omega = \frac{2V_E K_{BZ}}{\pi} \sin\frac{\pi}{2}\frac{K}{K_{BZ}}. \quad (1)$$

In Eq. (1), $V_E = (C_{ij}/\rho)^{1/2}$ is the acoustic wave velocity for the given propagation direction and polarization, C_{ij} is the corresponding elastic constant, ρ is the density, K is the wavevector magnitude, and K_{BZ} its value at the Brillouin zone boundary. According to Eq. (1) the frequency at the boundary is $\omega_{BZ} = (2/\pi)(C_{ij}/\rho)^{1/2}K_{BZ}$.

In a cubic material $\hbar\omega^*$ corresponds to ω_{BZ} for transverse waves propagating in the [100] direction. Thus the peak temperature in the $C_{p,\mathrm{lat}}/\beta T^3$ vs T curve is associated with C_{44}. Substituting values for C_{44}, ρ, and K_{BZ} ($=2\pi/a$, where a is the lattice parameter) in the above equation we find $\hbar\omega_{BZ} = \hbar\omega^* = 21.9$ meV. This frequency, which is indicated by the upward pointing arrow in Fig. 2, closely matches the value of $\hbar\omega$ where $d\omega/dK = 0$ in the measured phonon dispersion curves of Cu.

Figure 3 shows the $C_{p,\mathrm{lat}}/\beta T^3$ peak temperature versus $\hbar\omega^* = (2/\pi)(C_{\mathrm{shear}}/\rho)^{1/2}\ K_{BZ}$ for 12 cubic elements (4 bcc and 8 fcc, squares), 6 hcp elements (hexagons), 6 metallic glasses [solid dark circles (blue online)], and 3 oxide glasses [solid light gray circles (red online)] [18]. Data for one tetragonal alloy [open circle (blue online)] and two trigonal oxides [open circles (red online)] are also shown. All data were obtained from the literature, except that for $Pd_{40}Cu_{40}P_{20}$, which is our own. The abscissa of Fig. 3 corresponds to $\hbar\omega_{BZ}$ for shear waves propagating in the [100] direction. For a transverse wave in the [100] direction of fcc and bcc crystals $K_{BZ} = 2\pi/a$ (Γ to X in fcc, Γ to H in bcc) and $C_{\mathrm{shear}} = C_{44}$. For a transverse wave in the [100] direction in hexagonal and trigonal crystals, $K_{BZ} = 2\pi/(a\sqrt{3})$ (Γ to M) and for the fast shear wave $C_{\mathrm{shear}} = C' = (C_{11}-C_{12})/2$. For the glasses the boundary of the first pseudo-Brillouin zone was taken to be $K_{BZ} = Q_p/2$, where Q_p corresponds to the *first* sharp diffraction peak in the structure factor $S(Q)$ of metallic glasses [19,20] and the *second* peak in the $S(Q)$ of oxide glasses [19]. In elastically isotropic glasses, $C_{\mathrm{shear}} = C_{44}$.

The solid black line in Fig. 3 was fitted to the data for the 12 cubic elements (which have no optical phonons), and the dark and light gray (blue and red online) lines were

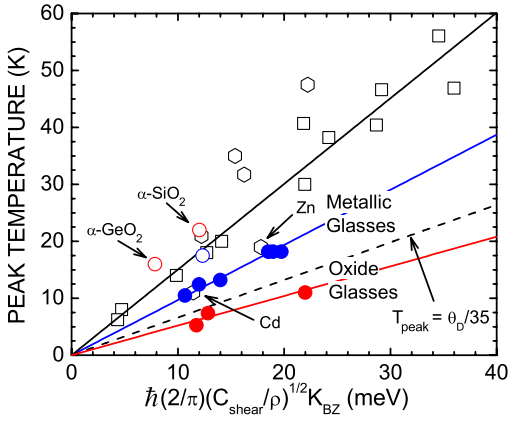

FIG. 3 (color online). Peak temperature vs $\hbar(2/\pi)(C_{\rm shear}/\rho)^{1/2}K_{BZ}$ for crystals and glasses. Left to right the materials are Cubic (squares): Kr [26], Ar [26], Au, Pt [27], Ag, Al [25,28], Cu, W, Ni, Mo, Cr, and Fe; hcp (hexagons): Cd [24,25], Zr, Mg, Re, Zn [24,25], and Ru [29]; Tetragonal [dark gray circle (blue online)]: $Pd_{40}Cu_{40}P_{20}$ [our data]; Trigonal [light gray circles (red online)]: α-GeO_2 [30,31], α-SiO_2 [1,32]; Metallic glasses [solid dark circles (blue online)]: $Pd_{77.5}Si_{16.5}Cu_6$ [33,34], $Pd_{40}Cu_{40}P_{20}$ [our data], $Zr_{41}Ti_{14}Cu_{12.5}Ni_{10}Be_{22.5}$ [35], $Fe_{40}Ni_{40}B_{20}$ [36,37], $Fe_{60}Ni_{40}B_{20}$ [36,37], and $Fe_{80}B_{20}$ [36,37]; Oxide glasses [solid light gray circles (red online)]: B_2O_3 [38,39], GeO_2 [40], SiO_2 [4,25,41]. Data not specifically referenced are from Refs. [25,32].

fitted to the data for the six metallic and the three oxide glasses, respectively. The dashed line plots $T_{\rm peak} = \theta_D/35$, which is predicted by the interstitialcy theory [11]. To construct this line we used Debye temperature and shear modulus data for the prototype metallic glass $Pd_{40}Ni_{40}P_{20}$ [21]. The data for the hcp elements (which have optical phonons) shows some scatter. However, these data show a trend: (1) the peak temperatures for Mg, Re, and Ru (which have optical branches above $\hbar\omega^*$) are greater than for cubic crystals, and (2) the peak temperatures of Cd and Zn (which have optical modes that lie mainly below ω^* [22,23] and thus hybridize with the acoustic modes) are lower than the peak temperatures for the cubic elements, and similar to the peak temperatures for the metallic glasses. Furthermore, in Cd and Zn the dispersion curves for transverse acoustic waves in the [100] and [110] directions have $d\omega/dK \cong 0$ singularities near the *middle* of the Brillouin zone and thus do not follow the dispersion relation given in Eq. (1). Both the optical modes and these *strongly dispersive* acoustic branches contribute to a high VDOS at low frequencies, certainly lower than the crossover frequency (Fig. 2).

We now address the magnitude of the $C_{p,\rm lat}/\beta T^3$ peak. The height of the peak in the $C_{p,\rm lat}/\beta T^3$ vs T/θ_D curve is related to the number of vibrational modes in *excess* of the Debye VDOS between zero frequency and ω^*. Let us consider this excess for Cu. For N atoms the number of Debye vibrational modes with $\omega \leq \omega^*$ is $N^D = 3N(\omega^*/\omega_D)^3$, where ω_D is the Debye frequency. Numerically integrating the area under the Cu VDOS up to ω^* we count approximately $1.7N$ modes. This was also the case for several other fcc crystals, whereas for bcc materials the value is $\sim 2N$ modes. Hence for cubic materials, the number of excess modes between 0 and ω^* is approximately $N^E = 1.85N – 3N(\omega^*/\omega_D)^3$.

The Debye frequency is determined mainly by the transverse acoustic phonons. We therefore take ω_D as proportional to the mean shear wave velocity, $\omega_D \propto [(C_{44}C')^{1/2}/\rho]^{1/2}$, where $(C_{44}C')^{1/2}$ is the mean shear modulus. Substituting the expressions for ω_D and ω^* into the equation for N^E, we find

$$N^E = 1.85N – 3N\gamma\left(\frac{C_{\rm shear}}{\sqrt{C_{44}C'}}\right)^{3/2}, \qquad (2)$$

where $\gamma = \text{const}$, $C_{\rm shear} = C_{44}$ for cubic crystals and glasses, and $C_{\rm shear} = C'$ for hcp and trigonal crystals.

Figure 4 is a plot of the peak amplitude (defined in Fig. 1) versus $[C_{\rm shear}/(C_{44}C')^{1/2}]^{3/2}$. That the data for cubic elements can be fitted with Eq. (2) (solid line) implies that the peak amplitude is indeed proportional to the number of excess modes. The data for the hcp elements, trigonal oxide crystals, and tetragonal $Pd_{40}Cu_{40}P_{20}$ crystal, however, clearly lie above the line for cubic materials and cannot be described by Eq. (2). This reflects the contributions of optical phonons and/or strongly dispersive acoustic phonon branches to the peak amplitude. The data for the metallic and oxide glasses also lie above the line for cubic crystals.

In summary, a peak in $C_{p,\rm lat}/T^3$ vs T is quite universal, appearing in crystalline as well as in amorphous materials. We have found that the temperature of the peak is related to the frequency where the Debye and actual VDOS cross for the first time. In hexagonal crystals the optical phonons and

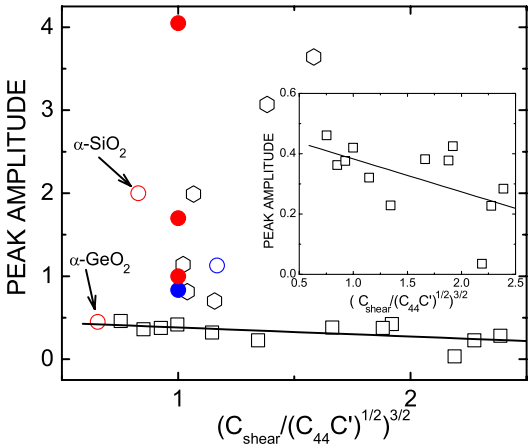

FIG. 4 (color online). Peak amplitude versus $[C_{\rm shear}/(C_{44}C')^{1/2}]^{3/2}$ for the same materials as in Fig. 3. Left to right the crystals are Cubic: Cr, Ar, Mo, W, Al, Pt, Kr, Fe, Ni, Au, Ag, and Cu; hcp: Mg, Ru, Re, Zr, Zn, and Cd; Trigonal: α-GeO_2 and α-SiO_2; Tetragonal: $Pd_{40}Cu_{40}P_{20}$. Top to bottom the glasses are SiO_2, GeO_2, B_2O_3, and $Pd_{40}Cu_{40}P_{20}$. Inset: Cubic elements.

the strongly dispersive acoustic phonon branches [which cannot be described by Eq. (1)] lower the temperature and increase the amplitude of the peak. In fact, the amplitude is larger than for cubic elements and metallic and oxide glasses [18]. Ostensibly, the foregoing analysis suggests that glasses also have low-frequency optical-like phonons and/or strongly dispersive acoustic phonon branches that contribute to the $C_{p,\mathrm{lat}}/T^3$ peak.

An alternative explanation for the $C_{p,\mathrm{lat}}/T^3$ peak is that the excess low-frequency states arise from resonant vibrational excitations associated with specific ''defects'' in glasses. For the resonant frequencies to be low, the defects should have a large effective mass and/or weak elastic restoring force. Two such defects are stringlike arrays identified by Schober and Oligschleger in molecular dynamic simulations of monatomic glasses [8] and interstitial pairs in dumbbell configuration proposed by Granato [11]. However, strings and interstitials in dumbbell configuration are not the only defects that could exist and be excited in glasses. Multicomponent bulk metallic glasses such as $Pd_{40}Cu_{40}P_{20}$ are characterized by weak metal-metal interatomic bonds and strong metal-metalloid bonds. In these glasses, the large discrepancy between bond strengths, the large difference between the masses of the metal and P atoms, and the presence of strong chemical short-range order (P atoms are surrounded only by metal atoms) should be conducive to low-frequency, breathing-type modes. Arguments could also be made that the atoms near regions of excess free volume in the glass are loosely bound and vibrate at relatively low frequencies. However, our measurements show that the temperature and amplitude of the $C_{p,\mathrm{lat}}/\beta T^3$ peak change little upon carefully annealing an as-quenched metallic glass.

The present analysis finds no clear distinction between the position and amplitude of the $C_{p,\mathrm{lat}}/T^3$ peak in crystals and the peak position and amplitude in *metallic* glasses. This is underscored by two observations: (1) the $C_{p,\mathrm{lat}}/T^3$ peak is *larger* in Cd and Zn than in glassy $Pd_{40}Cu_{40}P_{20}$ and (2) the peak amplitude for the $Pd_{40}Cu_{40}P_{20}$ single crystal is *larger* than for the $Pd_{40}Cu_{40}P_{20}$ *glass*. The latter result shows that the crystal has an even greater excess of low-frequency vibrational states than the glass of the same composition. Our analysis does suggest that the $C_{p,\mathrm{lat}}/T^3$ peak occurs at an anomalously low temperature in oxide glasses compared to metallic glasses or crystals. This implies that the excess vibrational (boson peak) modes have relatively lower frequencies in oxide glasses than in metallic glasses.

This work was funded by a LANL LDRD grant.

[1] R. C. Zeller and R. O. Pohl, Phys. Rev. B **4**, 2029 (1971).
[2] W. A. Phillips, J. Low Temp. Phys. **7**, 351 (1972).
[3] P. W. Anderson *et al.*, Philos. Mag. **25**, 1 (1972).
[4] *Amorphous Solids: Low Temperature Properties*, edited by W. A. Phillips (Springer, Berlin, 1981).
[5] V. K. Malinovsky *et al.*, Europhys. Lett. **11**, 43 (1990).
[6] F. J. Bermejo, A. Criado, and J. L. Martinez, Phys. Lett. A **195**, 236 (1994).
[7] U. Buchenau *et al.*, Phys. Rev. Lett. **53**, 2316 (1984).
[8] H. R. Schober and C. Oligschleger, Phys. Rev. B **53**, 11 469 (1996).
[9] D. A. Parshin, Phys. Solid State **36**, 991 (1994).
[10] W. Schirmacher *et al.*, Phys. Rev. Lett. **81**, 136 (1998).
[11] A. V. Granato, Physica (Amsterdam) **219–220B**, 270 (1996).
[12] A. V. Granato, J. Non-Cryst. Solids **307–310**, 376 (2002).
[13] E. S. R. Gopal, *Specific Heats at Low Temperatures* (Plenum Press, New York, 1966).
[14] R. M. Nicklow *et al.*, Phys. Rev. **164**, 922 (1967).
[15] Additional peaks in $C_{p,\mathrm{lat}}/\beta T^3$ vs T may occur, corresponding, for example, to the excitation of phonons in the $27 < \hbar\omega < 28$ meV range of Cu (diagonally hatched region, Fig. 2). Such a peak is not evident for Cu because (1) $C_{p,\mathrm{lat}}/\beta T^3$ decreases rapidly for $T/\theta_D > 0.1$, and (2) the number of excess modes in the range $27 < \hbar\omega < 28$ meV is small.
[16] L. van Hove, Phys. Rev. **89**, 1189 (1953).
[17] C. B. Walker, Phys. Rev. **103**, 547 (1956).
[18] We have peak temperature, elastic constant, and K_{BZ} data for only these six metallic and three oxide glasses. Reliable peak amplitude data are available for only one metallic glass.
[19] C. J. Benmore *et al.*, J. Phys. Condens. Matter **11**, 7079 (1999).
[20] M. Arai *et al.*, Philos. Mag. B **79**, 1733 (1999).
[21] E. F. Lambson *et al.*, Phys. Rev. B **33**, 2380 (1986).
[22] B. Dorner *et al.*, J. Phys. F **11**, 365 (1981).
[23] L. Almqvist and R. Stedman, J. Phys. F **1**, 785 (1971).
[24] T. C. Cetas *et al.*, Phys. Rev. **182**, 679 (1969).
[25] Y. S. Touloukian and E. H. Buyco, *Thermophysical Properties of Matter: Specific Heat* (Plenum Press, New York, 1970), Vol. 4–5.
[26] L. Finegold and N. E. Phillips, Phys. Rev. **177**, 1383 (1969).
[27] B. M. Boerstoel *et al.*, Physica (Amsterdam) **54**, 442 (1971).
[28] W. T. Berg, Phys. Rev. **167**, 583 (1968).
[29] G. T. Furukawa *et al.*, J. Phys. Chem. Ref. Data **3**, 163 (1974).
[30] A. P. Jeapes *et al.*, Philos. Mag. **29**, 803 (1974).
[31] M. Grimsditch *et al.*, J. Appl. Phys. **83**, 3018 (1998).
[32] G. Simmons and H. Wang, *Single Crystal Elastic Properties and Calculated Aggregate Properties: A Handbook* (MIT Press, Cambridge, 1971).
[33] H. S. Chen and W. H. Haemmerle, J. Non-Cryst. Solids **11**, 161 (1972).
[34] B. Golding *et al.*, Phys. Rev. Lett. **29**, 68 (1972).
[35] W. H. Wang *et al.*, Phys. Rev. B **62**, 25 (2000).
[36] D. G. Onn *et al.*, J. Appl. Phys. **52**, 1802 (1981).
[37] C.-P. Chou *et al.*, J. Appl. Phys. **50**, 3334 (1979).
[38] G. K. White *et al.*, Phys. Rev. B **29**, 4778 (1984).
[39] J. T. Krause and C. R. Kurkjian, *Borate Glasses*, edited by L. D. Pye, V. D. Frechette, and N. J. Kreidl (Plenum, New York, 1978), Vol. 12.
[40] A. A. Antoniou and J. A. Morrison, J. Appl. Phys. **36**, 1873 (1965).
[41] M. E. Fine *et al.*, J. Appl. Phys. **25**, 402 (1954).